Supplementary information

ATHENA: a dynamic metabolic hub balancing carbon economy and energy supply in microbial synthesis

Likun Guo[a], Xinjun Feng[b], Xingyu, Zhang[a], Chao Xu[c], Wei Liu[d], Yujia Bi[a], Qingsheng Qi[a], Mo Xian[c], Guang Zhao[a*]

[a] State Key Laboratory of Microbial Technology, Shandong University, Qingdao, 266237, China

[b] Research Center of Advanced Biological Manufacture, Dalian Institute of Chemical Physics, Chinese Academy of Sciences, Dalian, 116023, China

[c] CAS Key Laboratory of Biobased Materials, Qingdao Institute of Bioenergy and Bioprocess Technology, Chinese Academy of Sciences, Qingdao, 266101, China

[d] Guangzhou Institute of Energy Conversion, Chinese Academy of Sciences, Guangzhou, 510640, China

*correspondence: zhaoguang@sdu.edu.cn

Supplementary Tables

Supplementary Table 1. Stoichiometric analysis of basic and hybrid metabolic pathways.

Metabolism	Metabolites per mol glucose	AcCoA rank	NAD(P)H rank	ATP rank	C-yield
Basic					
EMP	2AcCoA+2CO_2+4NADH+2ATP	6	4	1	66.7%
PP	1.667AcCoA+2.667CO_2+3.333NADH+ 2NADPH+1.667ATP	8	1	3	55.6%
ED	2AcCoA+2CO_2+3NADH+1NADPH+1ATP	6	4	6	66.7%
NOG	3AcCoA-1ATP	1	9	12	100%
Hybrid					
PP+EMP	1.833AcCoA+2.333CO_2+3.667NADH+ 1NADPH+ 1.833ATP	7	2	2	61.1%
EMP+ED	2AcCoA+2CO_2+3.5NADH+0.5NADPH+ 1.5ATP	6	4	4	66.7%
PP+ED	1.833AcCoA+2.333CO_2+3.167NADH+ 1NADPH+1.333ATP	7	3	5	61.1%
NOG+EMP	2.5AcCoA+1CO_2+2NADH+0.5ATP	2	8	10	83.3%
NOG+PP	2.333AcCoA+1.333CO_2+1.667NADH+ 1NADPH+0.333ATP	3	7	9	77.8%
NOG+ED	2.5AcCoA+1CO_2+1.5NADH+0.5NADPH	2	8	11	83.3%
NOG+EMP+ PP	2.222AcCoA+1.556CO_2+2.444NADH+ 0.667NADPH+0.889ATP	4	5	7	74.1%
NOG+EMP+ ED	2.333AcCoA+1.333CO_2+2.333NADH+ 0.333NADPH+0.667ATP	3	6	9	77.8%
NOG+EMP+ PP+ED	2.167AcCoA+1.667CO_2+1.917NADH+ 0.75NADPH+0.75ATP	5	6	8	72.2%

Supplementary Table 2. Biochemical characterization of FrdABCD and NadB.

Category	FrdABCD	NadB
Subunit	four	single
Directionality	easily reversed	unidirectional
Location	inner membrane-bound	cytoplasmic soluble
ΔrG (kcal/mol)[a]	5.04	-38.58
NADH utilization	+	-

a: The Gibbs free energies of reactions were calculated at pH 7.3 and ionic strength 0.25.

Supplementary Table 3. Translational enhancers and naming in this study.

Translational enhancers	Sequence (5' → 3')	
rrn BoxA E. coli	GCUCUUUAACAA	T181Sf2
RecBoxA[a]	UUGUUAAAGAGC	T181Sf3
T4 gene 32	UUAAAUUAAAA	T181Sf4
rpsA E. coli	UUAAAUAUAAA	T181Sf5
tuf M. genitalium	UUAACAACAUAAUUU	T181Sf6
atpE E. coli	UUUUAACUGAAACAAA	T181Sf7
T7 gene10	UUUAACUUUAA	T181Sf8
Ω of TMV RNA	ACAAUUAC-repeats	T181Sf9

a: This translation enhancer does not exist naturally. It is an artificially constructed reverse complementary sequence of "*rrn BoxA E. coli*".

Supplementary Table 4. Stoichiometric parameters of ATHENA and previously reported carbon conservation pathways.

Pathway name	AcCoA	CO_2	NAD(P)H	ATP	C-yield	References
PGB	+2	+2	+4	0	66.7%	[1]
EP-bifido	+2.5	+1	+2	-1	83.3%	[2]
SCTPK	+3	0	0	-1	100%	[3]
NOG	+3	0	0	-1	100%	[4]
ATHENA	+4	-2	-2	-2	133%	

Supplementary Notes

Supplementary Note 1. Stoichiometry analysis of ATHENA.

First, one molecule of glucose is converted via upstream glycolysis into two molecules of phosphoenolpyruvate (PEP), as shown in equation (i). Subsequently, PEPs either continue into the downstream glycolysis catalyzed by PykF or enter the synthetic pathway catalyzed by Pck (Fig. 2a). By assuming that the PEP molecule entering the latter is *x*, the stoichiometry for the conversion of glucose into AcCoA, CO_2, NADH, and ATP could be calculated as shown in equation (ii). Then, (2-*x*) molecules of PEP proceed through the downstream glycolysis, yielding equation (iii). Therefore, the ATHENA could be calculated as equation (iv) ($x \in [0, 2]$).

$$C_6H_{12}O_6 \rightarrow 2\ PEP + 2\ NAD(P)H \quad (i)$$

$$x\ PEP + x\ HCO_3^- + 2x\ NAD(P)H + x\ ATP \rightarrow 2x\ AcCoA \quad (ii)$$

$$(2-x)\ PEP \rightarrow (2-x)\ AcCoA + (2-x)\ CO_2 + (2-x)\ NAD(P)H + (2-x)\ ATP \quad (iii)$$

$$C_6H_{12}O_6 \rightarrow (2+x)\ AcCoA + (2-2x)\ CO_2 + (4-3x)\ NAD(P)H + (2-2x)\ ATP,\ x \in [0,2] \quad (iv)$$

Then, the yields of AcCoA, CO_2, NAD(P)H, and ATP from glucose could be calculated as follows: $Y_{AcCoA/Glu} = 2+x$, $Y_{CO2/Glu} = 2-2x$, $Y_{NAD(P)H/Glu} = 4-3x$, $Y_{ATP/Glu} = 2-2x$. With an increase in *x*, $Y_{AcCoA/Glu}$ will increase, while $Y_{CO2/Glu}$, $Y_{NAD(P)H/Glu}$, and $Y_{ATP/Glu}$ will decrease. This indicates that the synthetic pathway features intrinsic energy consumption and high carbon yield. Hence, we designate it as the carbon conservation module (CCM) of ATHENA. Conversely, as *x* decreases, $Y_{AcCoA/Glu}$ will decrease, while $Y_{CO2/Glu}$, $Y_{NAD(P)H/Glu}$, and $Y_{ATP/Glu}$ will increase. This suggests that downstream glycolysis serve as an energy-producing but carbon-losing process. Therefore, we term it the energy generation module (EGM) of ATHENA.

Supplementary Note 2. Comparison of carbon conservation pathways.

According to the analysis in Supplementary Note 1, the carbon yield and energy status of ATHENA vary depending on the metabolic flux from the PEP node to CCM and EGM. Compared to previously reported carbon conservation pathways (Supplementary Table 4), ATHENA demonstrates superior potential, primarily manifested in three aspects. (1). ATHENA generates more energy when reaching the same theoretical carbon yield. (2). CCM incorporates carbon fixation reaction that enables continued CO_2 fixation while preventing carbon loss. Consequently, its theoretical carbon yield is higher than that of NOG and its variants, as these primarily prevent carbon loss. (3). AcCoA is the key precursor for the synthesis of numerous products, including fatty acids, alkanes, amino acids, alcohols and polyketides. The direct product of the CCM is AcCoA, not acetylphosphate produced by the PGB, EP-bifido, SCTPK and NOG, thus eliminating the need for additional enzymes to generate AcCoA through reversible reactions (e.g., the reversible reaction mediated by phosphotransacetylase that converts acetylphosphate to AcCoA).

Supplementary Figures

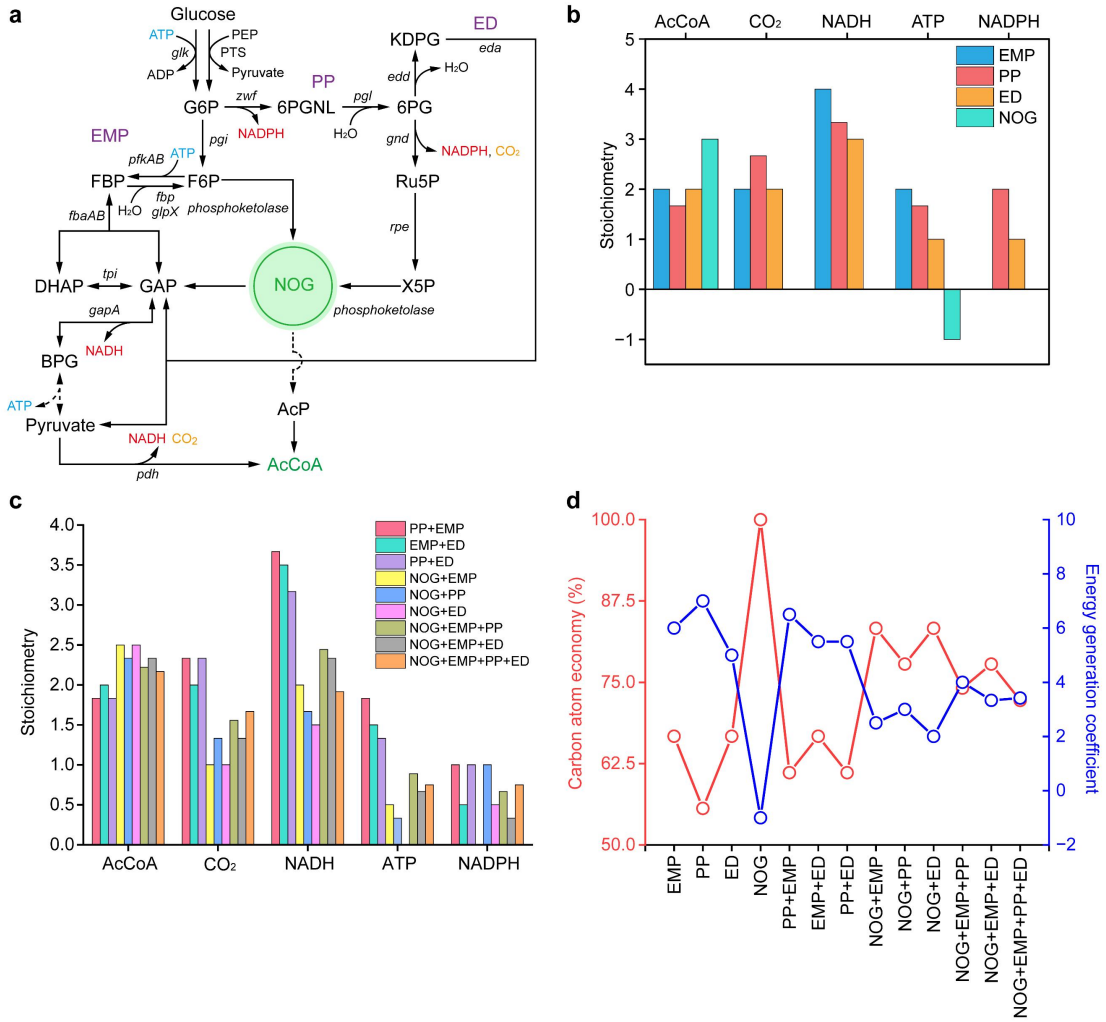

Supplementary Figure 1 Stoichiometric analysis of basic and hybrid metabolic pathways. a The configuration of three natural pathways (EMP, PP and ED) and one artificial pathway (NOG). G6P, glucose-6-phosphate; F6P, fructose-6-phosphate; FBP, fructose-1,6-biphosphate; AcP, acetylphosphate; DHAP, dihydroxyacetone phosphate; GAP, glyceraldehyde-3-phosphate; BPG, 1,3-biphospho-glycerate; AcCoA, acetyl-CoA; X5P, xylulose-5-phosphate; Ru5P, ribulose-5-phosphae; 6PG, gluconate 6-phosphate; 6PGNL, 6-phospho glucono-1,5-lactone; PEP, phosphoenolpyruvate; KDPG, 2-keto-3-deoxy-6-phosphogluconate; EMP, Embden-Meyerhof-Parnas; PP, Pentose Phosphate pathway; ED, Entner-Doudoroff pathway; NOG, non-oxidative glycolysis. **b** Stoichiometric coefficients of AcCoA, CO_2, NADH, ATP, and NADPH in the four fundamental metabolic pathways. **c** Stoichiometric coefficients of AcCoA, CO_2, NADH, ATP, and NADPH in the nine hybrid metabolic pathways, assuming glucose flux enters each pathway equally. **d** The performance of carbon atom economy and energy generation

coefficient in the basic and hybrid metabolic pathways. Carbon atom economy is represented by the ratio of carbon atoms in the product acetyl-CoA to those in glucose. The energy generation coefficient is expressed as the sum of the yield coefficients for NADH, NADPH, and ATP obtained per mole of glucose. Source data for this figure is available in the Source Data file.

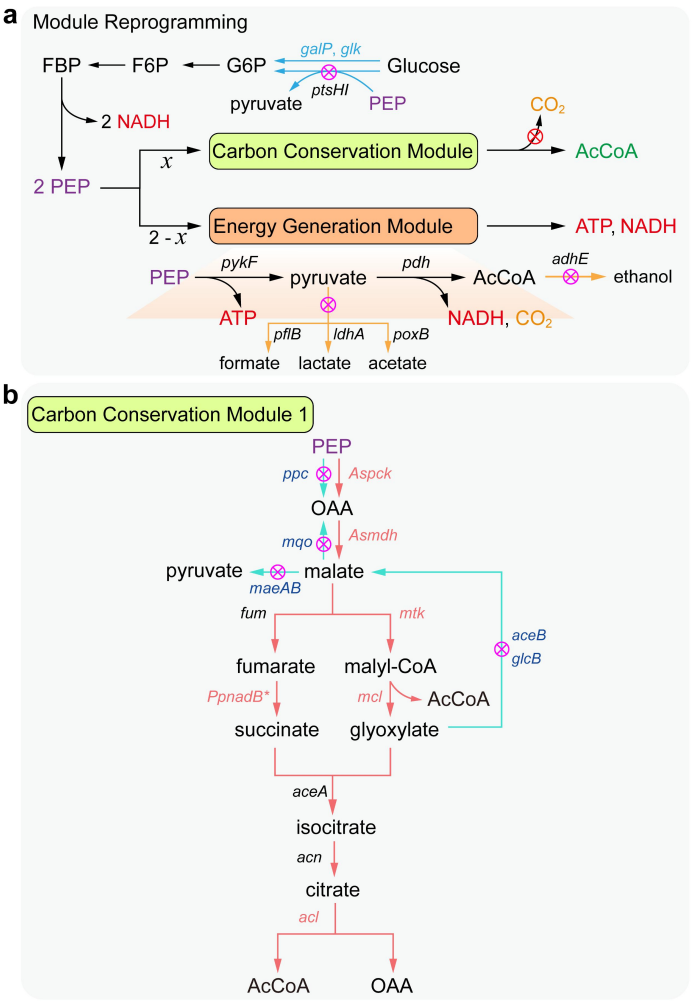

Supplementary Figure 2 Reprogramming of the central metabolic network. a The synthesis of AcCoA, ATP and NADH is divided into the carbon conservation module (CCM) and the energy generation module (EGM). **b** Construction of the CCM1. OAA, oxaloacetate. The complete pathway comprises the following: (1) The byproduct synthesis genes were knocked out, including *pflB*, *ldhA*, *adhE*, and *poxB*, thereby blocking the carbon loss; (2) The key PTS pathway genes *ptsHI* were replaced with *galP* and *glk* to avoid consumption of PEP; (3) The reverse synthesis pathway genes were knocked out, including *mqo*, *maeAB* and *ppc*. Additionally, *aceB* and *glcB* were knocked out to disrupt the futile cycle between malate and glyoxylate; (4) The genes related to the carbon conservation module were integrated.

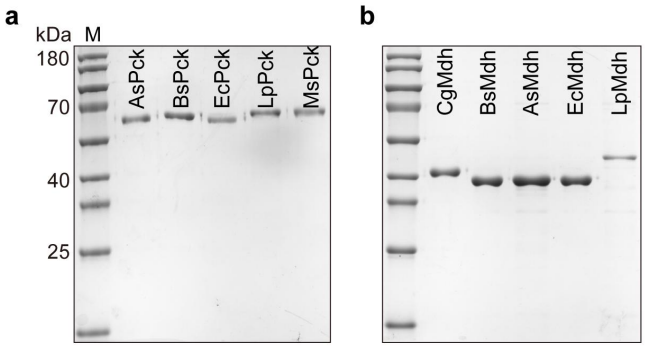

Supplementary Figure 3 SDS-PAGE of purified related enzymes. a phosphoenolpyruvate carboxykinase. **b** malate dehydrogenase. The phosphoenolpyruvate carboxykinase is derived from five different strains including *Actinobacillus succinogenes*, *Bacillus subtilis*, *Escherichia coli*, *Lactiplantibacillus plantarum* and *Mannheimia succiniciproducens*. The malate dehydrogenase is derived from five different strains including *Corynebacterium glutamicum*, *Bacillus subtilis*, *Actinobacillus succinogenes*, *Escherichia coli* and *Lactiplantibacillus plantarum*.

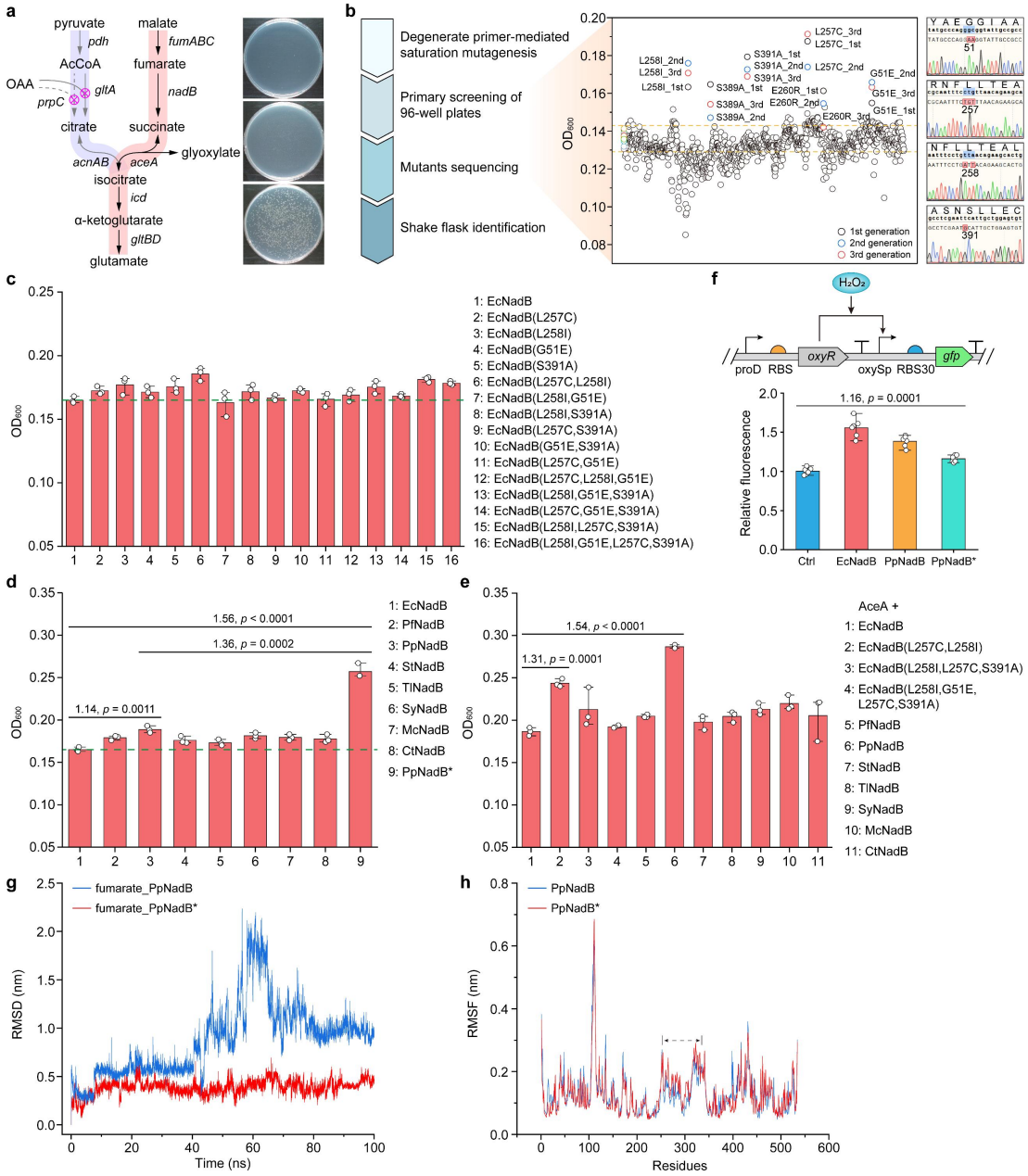

Supplementary Figure 4 A genetic selection system based on glutamate availability for screening aspartate oxidase. a Schematic diagram of the growth-coupled glutamate auxotrophy-based genetic screening system. The glutamate-auxotrophic mutant (knockout of *gltA* and *prpC*) was barely grown in a minimal medium plate (inner top image). Overexpressing the *nadB* in the mutant, small colonies were grown (middle). Colony size increased with further addition of glutamate (bottom). **b** The screening process. The orange dashed line indicated the growth detection range for the unmutated control strain. **c** Screening of single and combination point mutations in *nadB* from *E. coli* (EcNadB) in shake flasks (n = 3 biological independent samples). **d** Growth of the glutamate-auxotrophic mutant expressing eight different strains-derived

nadB genes (n = 3 biological independent samples). The strains include *E. coli*, *Piromyces finnis* (Pf), *Pseudomonas putida* (Pp) and its mutant PpNadB L257C/L258I (PpNadB*), *Sulfolobus tokodaii* (St), *Thermococcus litoralis* DSM 5473 (Tl), *Synechocystis* sp. PCC 6803 (Sy), *Methylococcus capsulatus* (Mc) and *Chlorobium tepidum* (Ct). **e** The effect of overexpressing isocitrate lyase gene *aceA* and *nadB* on the mutant growth (n = 3 biological independent samples). **f** The H_2O_2 production was detected using a H_2O_2 biosensor to monitor the reaction between NadB and oxygen (n = 6 biological independent samples). PpNadB* reduced reactivity with oxygen. RMSD of fumarate for PpNadB and PpNadB* (**g**) and RMSF analysis for PpNadB and PpNadB* (**h**). The black dashed line denotes the substrate tunnel region. Values are presented as mean ± SD. Two-tailed Student's *t* tests were performed to determine the statistical significance. Source data for this figure is available in the Source Data file.

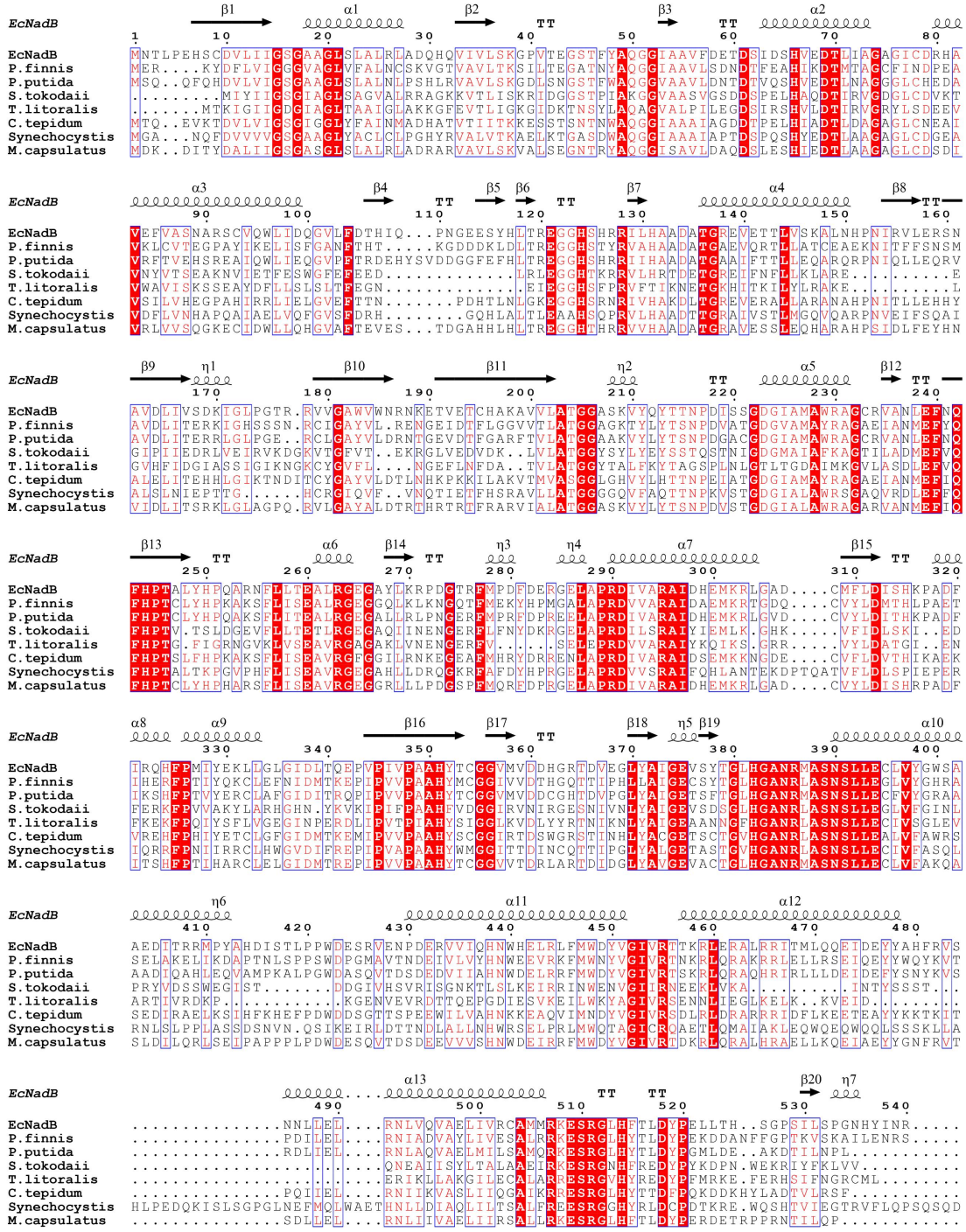

Supplementary Figure 5 Sequence alignment of the aspartate oxidase. The aspartate oxidase from *Escherichia coli* was aligned with other seven which were from *Piromyces finnis*, *Pseudomonas putida*, *Sulfolobus tokodaii*, *Thermococcus litoralis* DSM 5473, *Chlorobium tepidum*, *Synechocystis* sp. PCC 6803 and *Methylococcus capsulatus*, respectively.

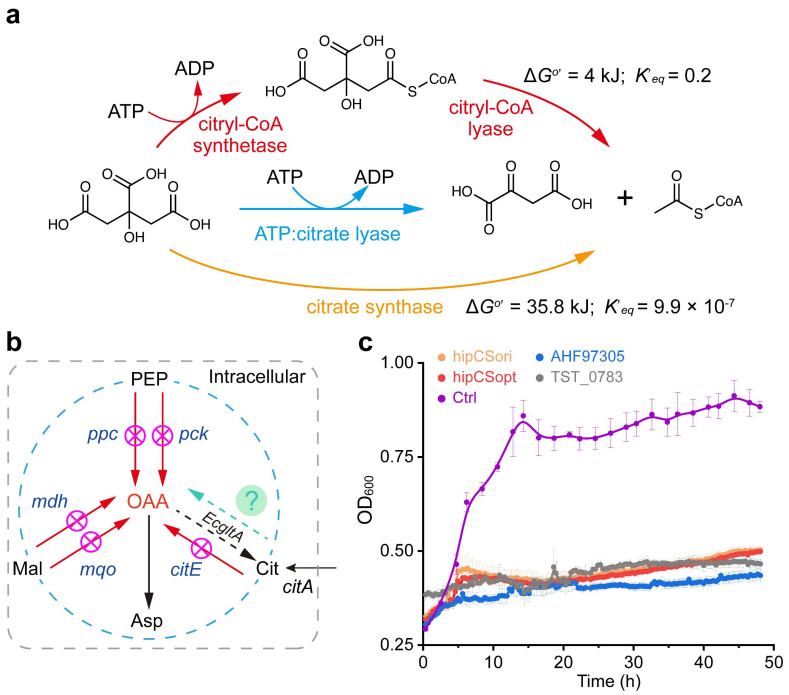

Supplementary Figure 6 The functional validation of ATP-independent citrate synthase in CCM1. a Three primary pathways for citrate cleavage into oxaloacetate and AcCoA. These pathways involve the following: under the catalysis of citrate-CoA synthase (CCS), ATP is involved to generate citrate-CoA. Subsequently, citrate lyase (CCL) catalyzes the formation of oxaloacetate and AcCoA; Citrate is converted via the ATP-dependent lyase Acl or ATP-independent citrate synthase. **b** Determine whether citrate synthase functions by constructing an oxaloacetate-auxotrophic mutant. Genes involved in the endogenous production of oxaloacetate in *Escherichia coli* (*ppc*, *pck*, *mdh*, *mqo*, and *citE*) were knocked out. 5 mM of citrate was added, and the citrate transporter gene *citA* was overexpressed. PEP, phosphoenolpyruvate; OAA, oxaloacetate; Mal: malate; Asp, aspartate; Cit: citrate. **c** Growth assay of the strain overexpressing citrate synthase in minimal medium. The control strain expressed the ATP-dependent citrate lyase from *Chlorobium tepidum*. Previously reported ATP-independent citrate synthase genes were synthesized and overexpressed, including $hipCS_{ori}$ from *Hippie maritima* and its codon-optimized gene $hipCS_{opt}$, *TST_0783* from *Thermosulfidibacter takaii*, and *AHF97305* from *Desulfurella acetivorans*. Values are presented as mean ± SD (n = 3 biological independent samples). Source data for this figure is available in the Source Data file.

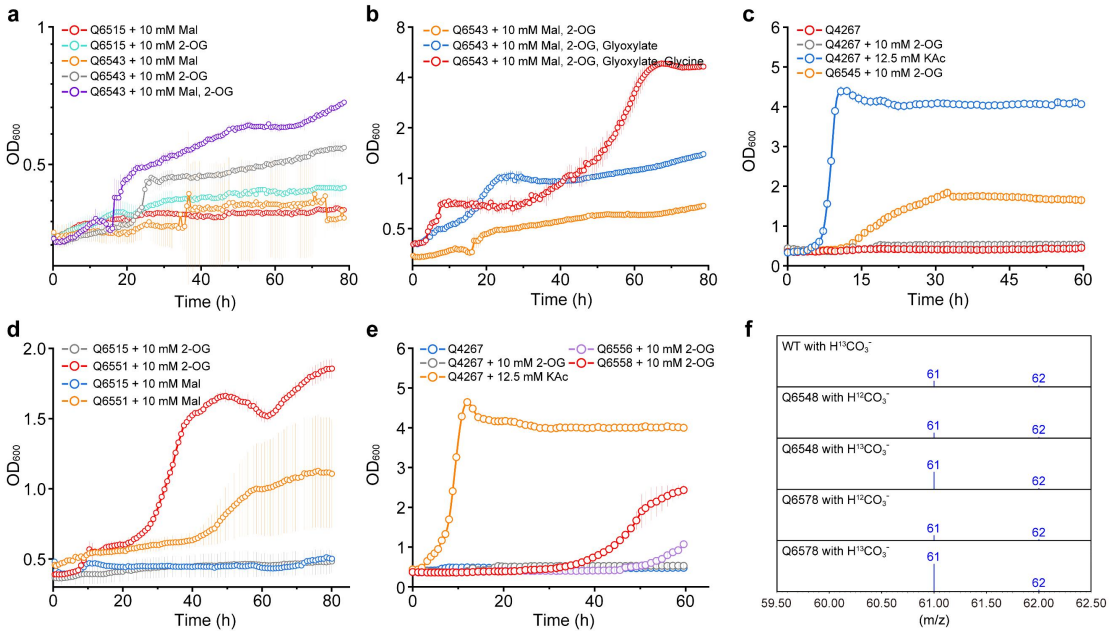

Supplementary Figure 7 Exploring the optimization clues of carbon conserving module 2 (CCM2). a In vivo validation of CCM2 based on oxaloacetate availability. Q6515 is oxaloacetate-auxotrophic BW25113 mutant, and Q6543 was generated by introduction of a partial CCM2 (excluding *pck* and *mdh*) and dicarboxylate transporter DctP into Q6515 (n = 3 biological independent samples). **b** Improvement of strain Q6543 growth by supplementation of glyoxylate and glycine (n = 3 biological independent samples). In vivo validation of CCM2 with enhanced glyoxylate supply (Supplementary Figs. 8 and 9) based on acetyl-CoA (**c**) and oxaloacetate (**d**) availability (n = 3 biological independent samples). **e** Enhancing aspartate-glyoxylate aminotransferase gene *bhcA* expression could improve the performance of CCM2. (n = 3 biological independent samples). **f** Mass spectrum of acetate produced by BW25113 wild strain, Q6548 and Q6578 with ^{12}C- or ^{13}C-labeled HCO_3^-. The m/z of 61 indicated that a ^{13}C atom was incorporated. Mal, malate; 2-OG, 2-oxoglutarate; KAc, potassium acetate. Values are presented as mean ± SD. Source data for this figure is available in the Source Data file.

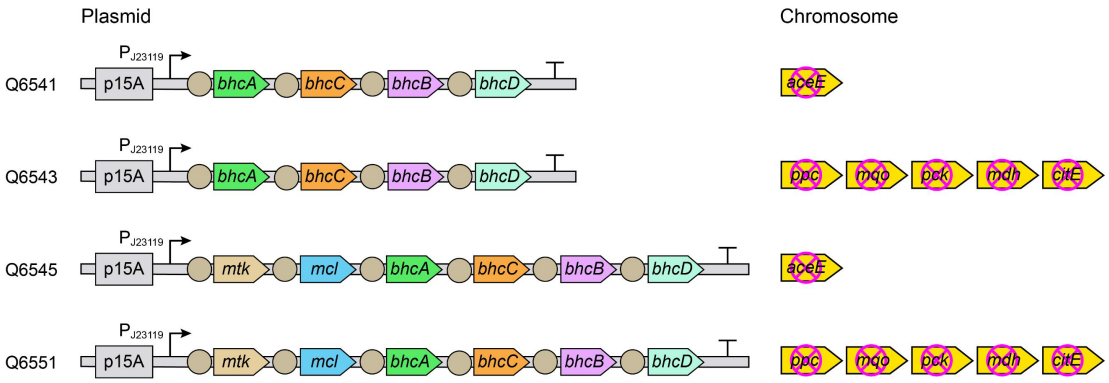

Supplementary Figure 8 Introduction and optimization of the CCM2 in acetyl-CoA-auxotrophic and oxaloacetate-auxotrophic strains to achieve glyoxylate recycling. In the acetyl-CoA auxotrophic strain, the endogenous *aceE* gene was knocked out. In the oxaloacetate-auxotrophic strain, the endogenous *ppc*, *mqo*, *pck*, *mdh* and *citE* were knocked out. In strains Q6545 and Q6551, the Mtk and Mcl genes were overexpressed to further enable glyoxylate supply.

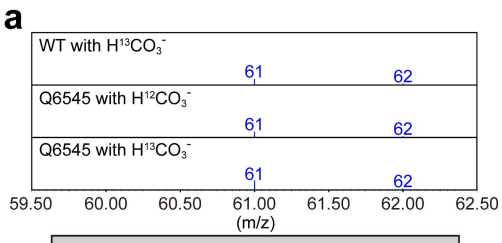

m/z of Acetic acid	61	62
Natural abundance	2.93%	0.41%
WT with $H^{13}CO_3^-$	2.80%	0.44%
Q6545 with $H^{12}CO_3^-$	2.57%	0.42%
Q6545 with $H^{13}CO_3^-$	4.40%	0.46%

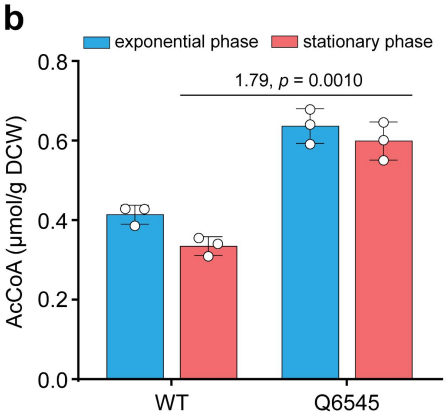

Supplementary Figure 9 Verification of CO_2 fixation and determination of acetyl-CoA concentration in Q6545. a CO_2 fixation validated by stable isotope labelling. Strain Q6545 was cultured in minimal medium supplemented with ^{12}C- or ^{13}C-labeled HCO_3^-. Mass spectrum and percentage of acetate with different m/z produced by each strain were presented. The m/z of 61 indicated that a ^{13}C atom was incorporated. **b** The intracellular acetyl-CoA concentration of BW25113 (WT), Q6545. Values are presented as mean ± SD (n = 3 biological independent samples). Two-tailed Student's *t* tests were performed to determine the statistical significance. Source data for this figure is available in the Source Data file.

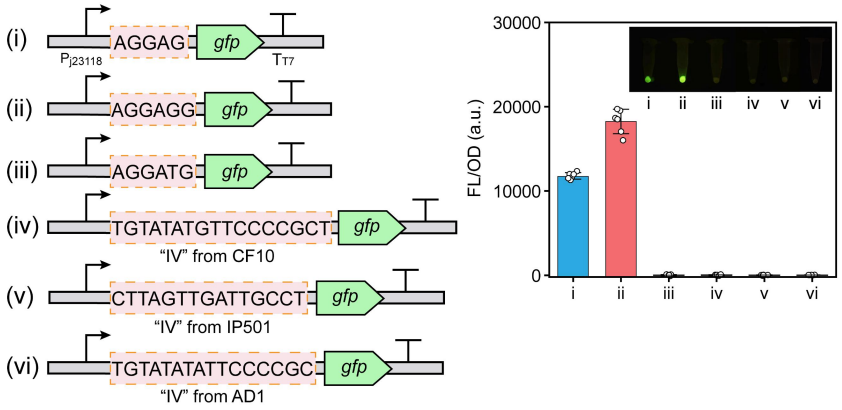

Supplementary Figure 10 Translation efficiency detection for different sequences. The sequences include “AGGAG”, “AGGAGG”, “AGGATG” and segments IV from different transcription attenuators. Values are presented as mean ± SD (n = 6 biological independent samples). Source data for this figure is available in the Source Data file.

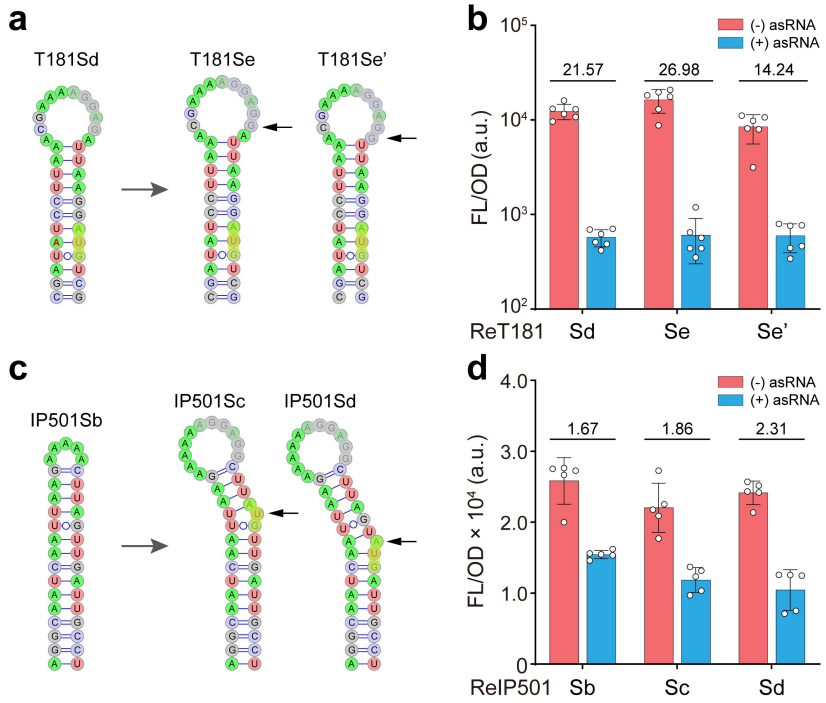

Supplementary Figure 11 Different incorporation methods of translation components and detection of repression effects. Insertion of a ribosomal-binding site and a start codon within the terminator hairpins of pT181 (**a**) and pIP501 (**c**). The repression induced by antisense RNA in the modified pT181 (**b**) (n = 6 biological independent samples) and pIP501 (**d**) (n = 5 biological independent samples). Values are presented as mean ± SD. Source data for this figure is available in the Source Data file.

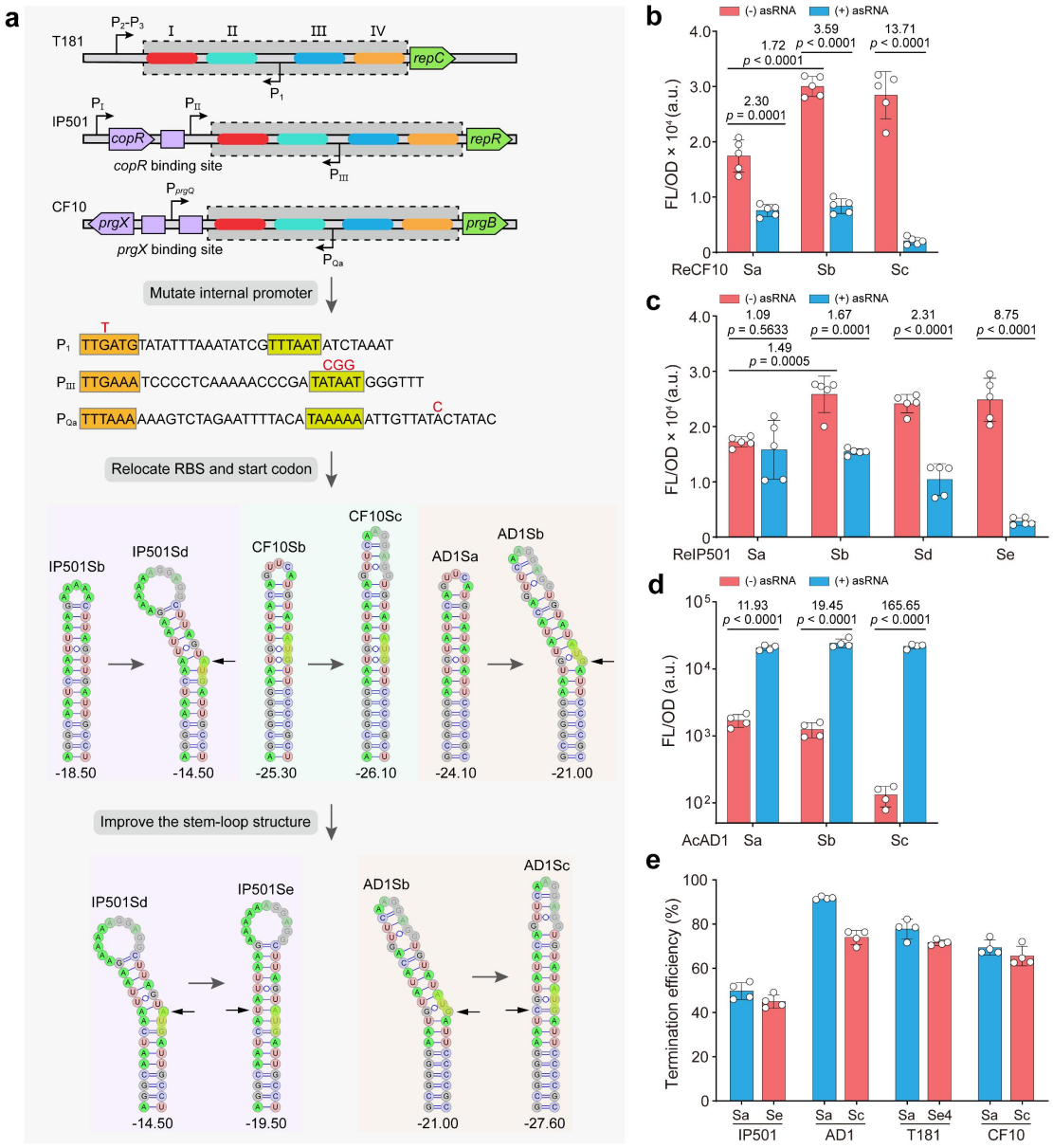

Supplementary Figure 12 Construction of asRNA-mediated regulatory devices based on transcription attenuator pCF10, pIP501 and pAD1. a Optimization process. The secondary structure of each sense target RNA was shown. Red bases indicate the mutated sequences and the numbers represent the free energy (kcal/mol) The brown and yellow areas denote -35 and -10 regions, respectively. The responsive characteristics of sense targets derived from ReCF10Sa (**b**) (n = 5 biological independent samples), ReIP501Sa (**c**) (n = 5 biological independent samples) and AcAD1Sa (**d**) (n = 4 biological independent samples). **e** Termination efficiency of intrinsic terminators in attenuators before and after modification (n = 4 biological independent samples). Values are presented as mean ± SD. Two-tailed

Student's *t* tests were performed to determine the statistical significance. Source data for this figure is available in the Source Data file.

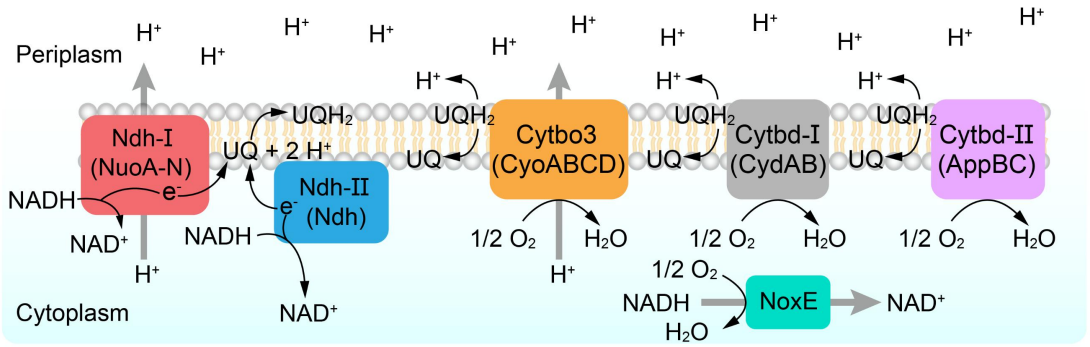

Supplementary Figure 13 Schematic diagram of the *E. coli* respiratory chain. The natural respiratory chain of *E. coli* is regulated by five gene clusters, including *nuoA-N*, *ndh*, *cyoABCD*, *cydAB* and *appBC*. The NADH oxidase encoded by *noxE* was introduced into *E. coli* to consume NADH for regulating the intracellular redox environment.

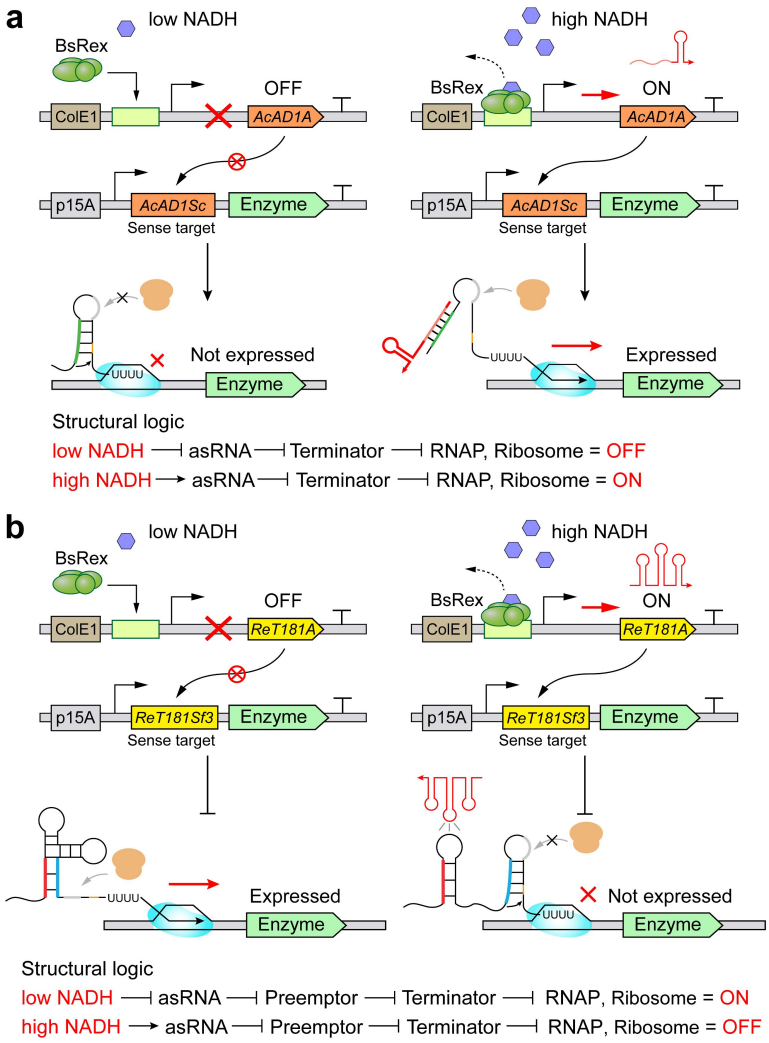

Supplementary Figure 14 Detailed process diagram of the NADH-responsive asRNA-mediated regulatory network during changes in the intracellular redox environment. When intracellular NADH level is low, the asRNA AcAD1A cannot be transcribed, causing cognate target AcAD1Sc to adopt a closed conformation and inhibiting downstream enzymes. When NADH level is high, AcAD1A transcription occurs, causing AcAD1Sc to adopt an open conformation and activating downstream enzymes. Collectively, for the AcAD1A and AcAD1Sc RNA pairs, as intracellular NADH level increases, the downstream enzyme transitions from a non-expressed state to an activated, expressed state (**a**). For asRNA ReT181A and its regulated sense RNA ReT181Se4, the opposite pattern occurs. As intracellular NADH level rises, the downstream enzyme transition from an expressed state to an inhibited, non-expressed state (**b**).

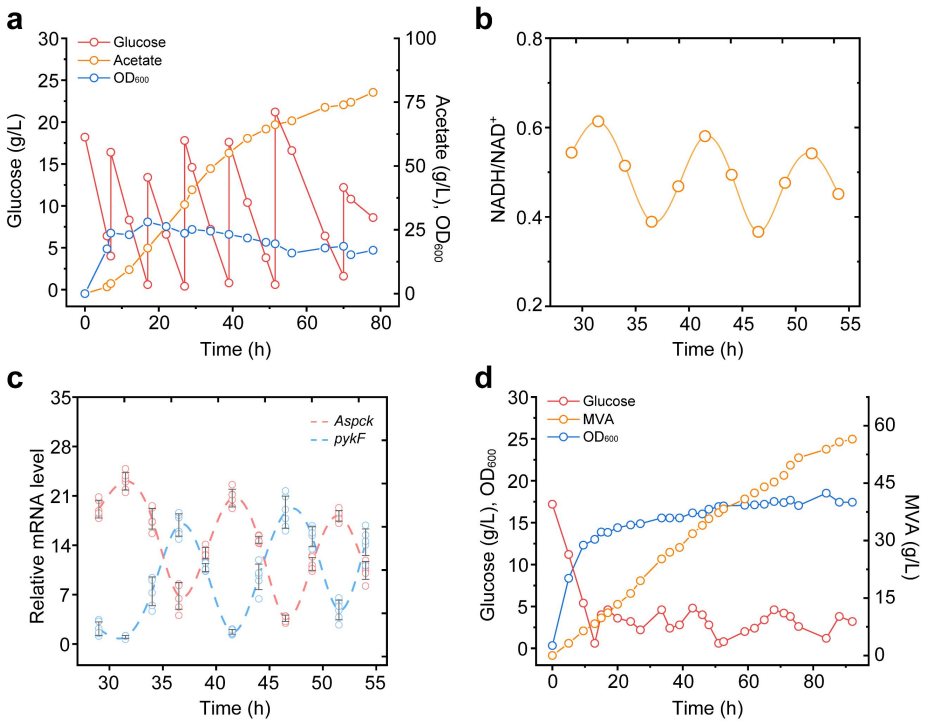

Supplementary Figure 15 Fermentation characterization in the 5-L bioreactor. a Time profiles for cell growth, residual glucose and acetate production during an aerobic fed-batch fermentation of strain Q6549-Ac in a 5-L bioreactor. **b-c**. The intracellular NADH/NAD$^+$ (**b**) and relative mRNA level of *Aspck* and *pykF* (**c**) of strain Q6549-Ac during acetate fed-batch fermentation. **d** Time profiles for cell growth, residual glucose and MVA production during an aerobic fed-batch fermentation of strain Q6549-MVA in a 5-L bioreactor. Source data for this figure is available in the Source Data file.

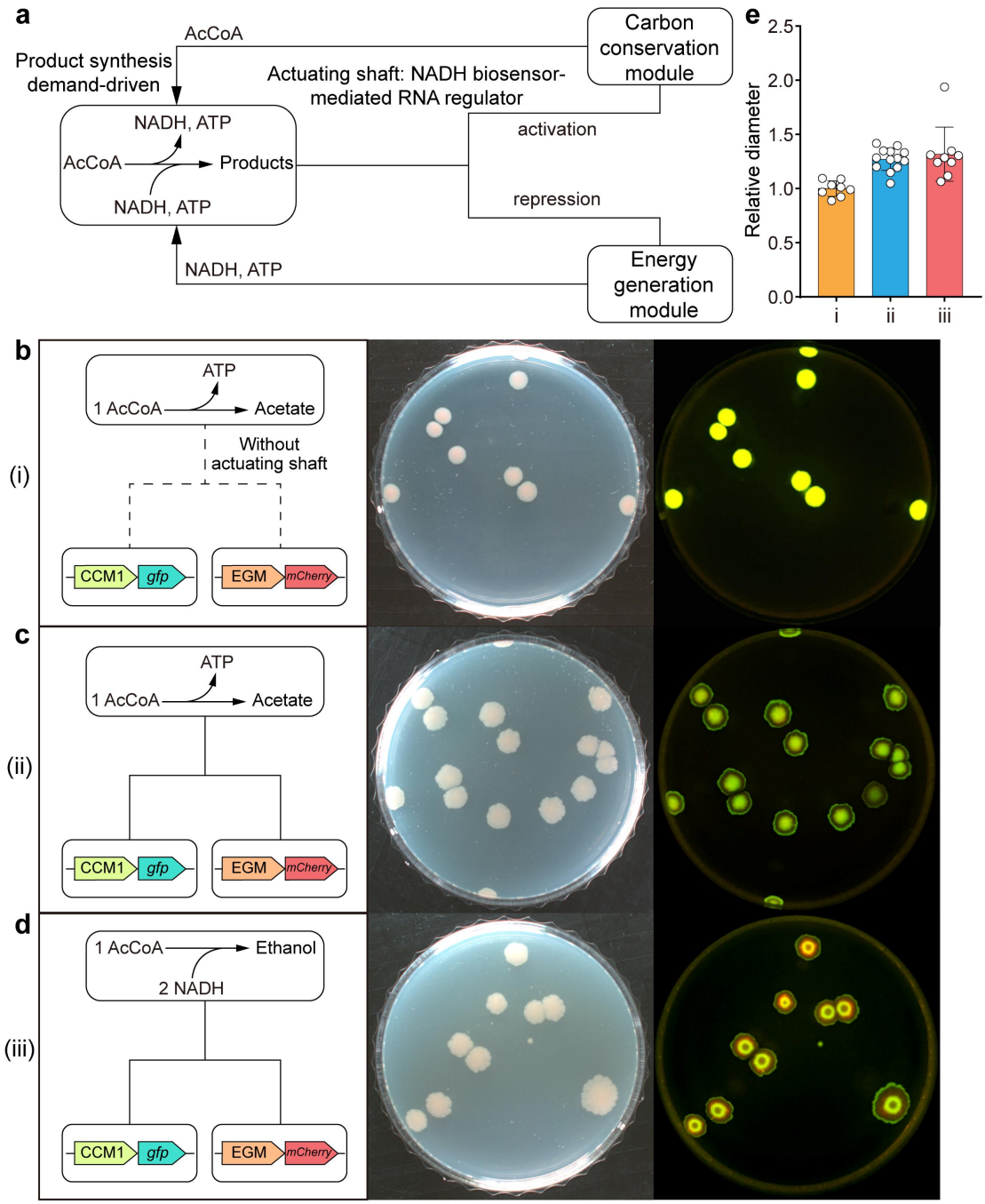

Supplementary Figure 16 Spatial distribution patterns of ATHENA. a Redox-driven dynamic regulation of a carbon conservation–energy generation closed loop. Introduction of product synthesis pathways for energy-generating or energy-consuming drives the shifts of the intracellular NADH/NAD^+. These redox changes were transmitted through the actuating shaft-an NADH biosensor-mediated asRNA regulatory system-as cascade feedback to the carbon conservation module CCM1 and energy generation module EGM, which supply AcCoA and energy respectively for the product synthesis pathways, thus forming a closed regulatory loop. **b** Introducing the acetate

synthesis pathway of energy generation but lacking the actuating shaft (i). **c** Introducing the acetate synthesis pathway of energy generation (ii). **d** Introducing the ethanol synthesis pathway of energy consumption (iii). In i-iii, CCM1 and EGM were characterized using green fluorescent protein GFP and red fluorescent protein mCherry, respectively. **e** Relative diameter measurement of colonies in plates. The smaller colony size of strain i may be attributed to the simultaneous overexpression of CCM1 and EGM genes, resulting in excessive metabolic burden. Source data for this figure is available in the Source Data file.

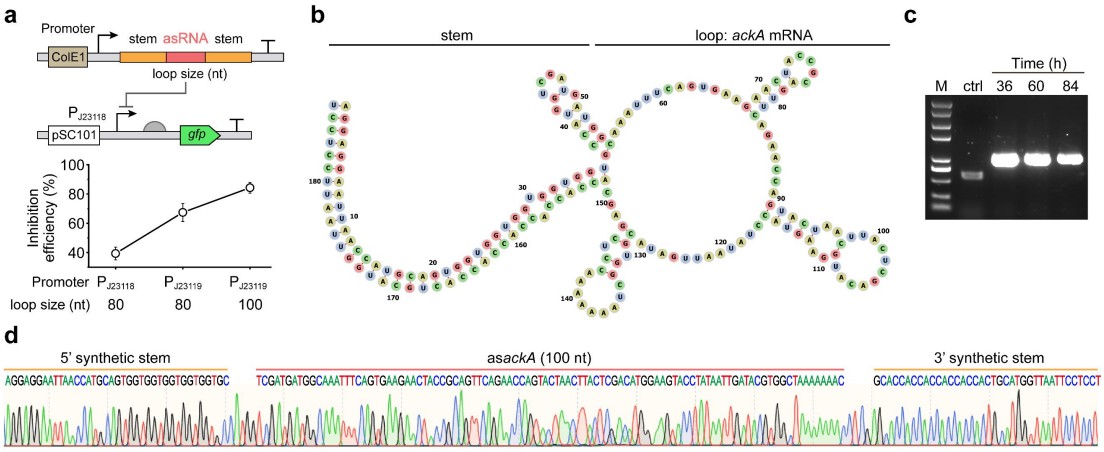

Supplementary Figure 17 The asRNA repression strategy based on artificial paired stems structure was employed to inhibit the *ackA* gene of *E. coli*. **a** Determining the effect of different bioparts on antisense RNA repression properties (n = 3 biological independent samples). The target gene *ackA* inhibited with 100-nt asRNA transcribed by promoter P_{J23119} was considered to possess strong repression. The 80-nt asRNA with P_{J23119} or P_{J23118} promoter respectively was considered to exhibit moderate or weak repression. Values are presented as mean ± SD. **b** The secondary structures of 100-nt *ackA* asRNA with the paired stems. **c** PCR analysis of samples at 36, 60, and 84 h of fermentation. The control lacking asRNA repression sequence was 567-bp, while samples containing it was 999-bp. **d** The PCR product of 84-hour fermentation culture was sequenced and no base mutations were found. Source data for this figure is available in the Source Data file.

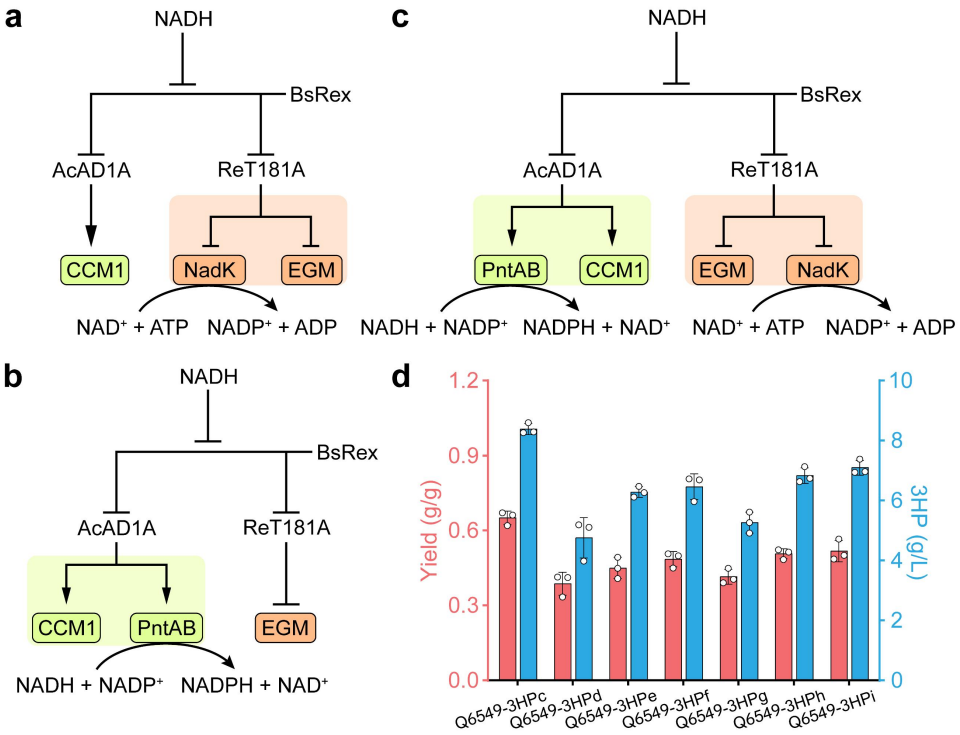

Supplementary Figure 18 Increase NADH or/and NAD⁺ transformation to investigate whether this could further promote 3HP synthesis. ATHENA involving dynamic regulation of *nadK* (**a**), *pntAB* (**b**), *pntAB* and *nadK* (**c**), respectively, based on the Q6549-3HPc strain, generating strains Q6549-3HPg, Q6549-3HPh, and Q6549-3HPi. Specifically, *pntAB* coordinate with CCM1, both of which are positively regulated by the NADH biosensor-mediated RNA regulators. When intracellular NADH is high, CCM1 is activated and PntAB promotes the conversion of NADH to NADPH. Consumption of NADH represses CCM1 and *pntAB*, while upregulating EGM and *nadK*. EGM enhances NADH production, while NadK promotes the transformation of NAD^+ into $NADP^+$. **d** 3HP titer and yield. Constitutive expression of *nadK*, *pntAB*, *nadK* and *pntAB*, respectively, based on the Q6549-3HPc, generating strains Q6549-3HPd, Q6549-3HPe, and Q6549-3HPf. Values are presented as mean ± SD (n = 3 biological independent samples). Source data for this figure is available in the Source Data file.

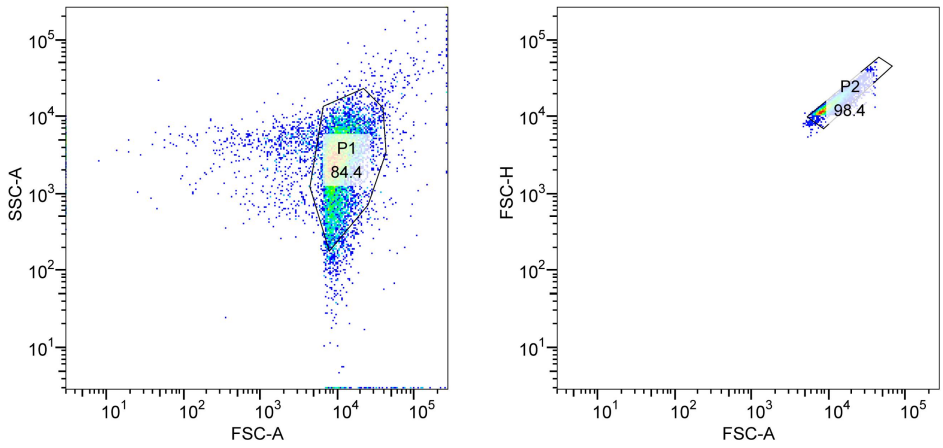

Supplementary Fig. 19 Events were gated to reduce false events in flow cytometry analysis.

Supplementary References

1. Opgenorth, P. H., Korman, T. P. & Bowie, J. U. A synthetic biochemistry module for production of bio-based chemicals from glucose. *Nat Chem Biol* **12**, 393-395 (2016).

2. Wang, Q. *et al.* Engineering an in vivo EP-bifido pathway in *Escherichia coli* for high-yield acetyl-CoA generation with low CO_2 emission. *Metab Eng* **51**, 79-87 (2019).

3. Guo, L. *et al.* Using a synthetic machinery to improve carbon yield with acetylphosphate as the core. *Nat Commun* **14**, 5286 (2023).

4. Bogorad, I. W., Lin, T. S. & Liao, J. C. Synthetic non-oxidative glycolysis enables complete carbon conservation. *Nature* **502**, 693-697 (2013).

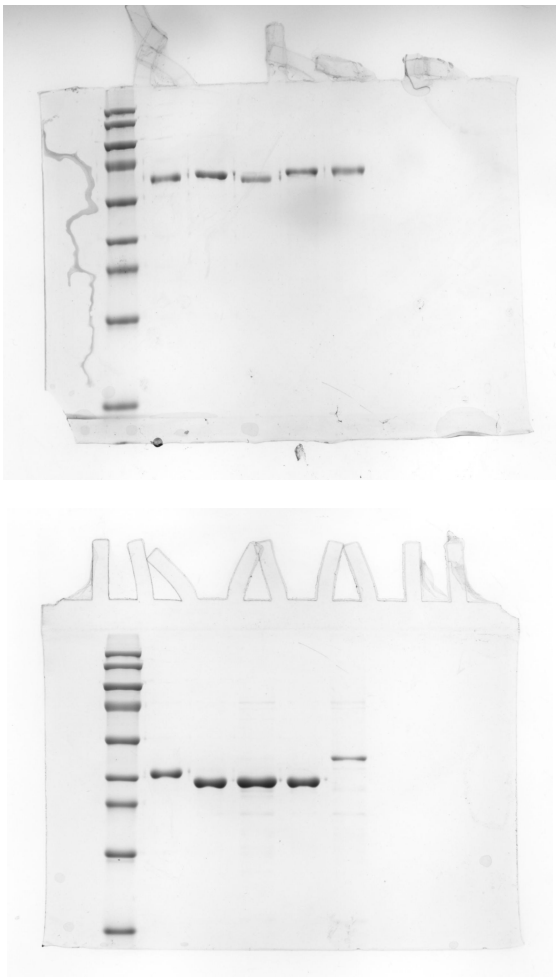

Uncropped gel for Supplementary Figure 3

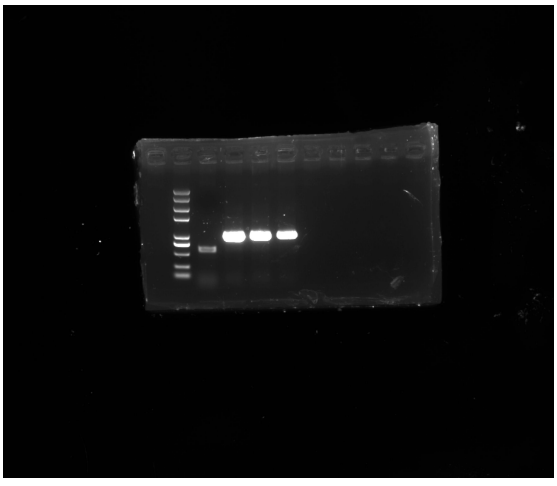

Uncropped gel for Supplementary Figure 17c